Climate Dynamics manuscript No.
(will be inserted by the editor)

Potential for seasonal prediction of Atlantic sea surface temperatures using the RAPID array at 26°N

A. Duchez* · P. Courtois* · E. Harris · S. A. Josey · T. Kanzow · R. Marsh · D. A. Smeed · J. J.-M. Hirschi

Received: date / Accepted: date

Abstract The Atlantic meridional overturning circulation (AMOC) plays a critical role in the climate system and is responsible for much of the meridional heat transported by the ocean. In this paper, the potential of using AMOC observations from the 26°N RAPID array

Corresponding author: A. Duchez,
National Oceanography Centre, European Way, Southampton, SO14 3ZH, UK.
E-mail: A.Duchez@noc.ac.uk

P. Courtois,
Department Earth and Atmospheric Sciences, University of Alberta, Edmonton, Alberta, Canada.
E-mail: courtoispeggy@gmail.com

J. J.-M. Hirschi,
National Oceanography Centre, Southampton, UK.
E-mail: joel.hirschi@noc.ac.uk

E. Harris,
Ariel Re BDA Limited, 31 Victoria Street, Hamilton HM 10, Bermuda.
E-mail: Elizabeth.Harris@arielre.com

S. Josey,
National Oceanography Centre Southampton, UK.
E-mail: simon.josey@noc.ac.uk

T. Kanzow,
Alfred-Wegener-Institute, Helmholtz Centre for Polar and Marine Research, Bremerhaven, Germany.
E-mail: torsten.kanzow@awi.de

R. Marsh,
Ocean and Earth Science, University of Southampton, UK.
E-mail: trobert.marsh@noc.soton.ac.uk

D. Smeed,
National Oceanography Centre, Southampton, UK.
E-mail: das@noc.ac.uk

to predict North Atlantic sea surface temperatures is investigated for the first time. Using spatial correlations and a composite method, the AMOC anomaly is used as a precursor of North Atlantic sea–surface temperature anomalies (SSTAs). The results show that the AMOC leads a dipolar SSTA with maximum correlations between two and five months. The physical mechanism explaining the link between AMOC and SSTA is described as a seesaw mechanism where a strong AMOC anomaly increases the amount of heat advected north of 26°N as well as the SSTA, and decreases the heat content and the SSTA south of this section. In order to further understand the origins of this SSTA dipole, the respective contributions of the heat advected by the AMOC versus the Ekman transport and air–sea fluxes have been assessed. We found that at a 5–month lag, the Ekman component mainly contributes to the southern part of the dipole and cumulative air–sea fluxes only explain a small fraction of the SSTA variability. Given that the southern part of the SSTA dipole encompasses the main development region for Atlantic hurricanes, our results therefore suggest the potential for AMOC observations from 26°N to be used to complement existing seasonal hurricane forecasts in the Atlantic.

Keywords Atlantic Meridional Overturning Circulation · RAPID array · Seasonal potential predictability · Sea Surface Temperature · Air–sea heat flux

1 Introduction

The Atlantic Meridional Overturning Circulation (AMOC), consists of a net northward flow of warm water in the upper ocean (typically in the top 1000m), which is compensated at greater depths by a cold southward return flow (e.g. Trenberth and Caron (2001), Ganachaud and Wunsch (2002), Wunsch (2005)). The AMOC has long been used in order to investigate the origin of interannual to decadal variability in the climate system. Indeed, both observational and modelling studies support the idea that the decadal climate variability in the North Atlantic has been closely related to the AMOC (e.g. Gordon et al (1992), Winton (2003), Latif et al (2004), Herweijer et al (2005)). Consequently, several climate predictability studies focused on, first, trying to predict the AMOC **(Matei et al (2012), Pohlmann et al (2013))** and second, assessing its impact on climate (Collins and Sinha (2003), Keenlyside et al (2008), Msadek et al (2010), Robson et al (2012a), Persechino et al (2013), Robson et al (2014)).

Interest in the AMOC has been stimulated by the prospect of its gradual weakening during the 21^{st} century as suggested by the climate model scenarios of the 4th and 5th Intergovernmental Panel on Climate Change (IPCC) assessment reports (Solomon et al (2007), Stocker et al (2013)). Climate model forecasts suggest a decline of the AMOC by 25% over the next few decades Bindoff et al (2007). **Over the past decade, a decrease in the subtropical AMOC has been observed (Smeed et al (2014)) in addition to increased Atlantic sea–surface temperatures (SSTs) (Buchan et al (2014)), and an upward trend in Atlantic hurricanes has been observed since 1995 (Goldenberg et al (2001), Emanuel (2005), Sriver and Huber (2007), Klotzbach and Gray (2008), Strazzo et al (2013))**. A possible degree of causality exists between these processes and indicates that measuring the large scale ocean circulation could be a useful tool in assessing seasonal hurricane formation probabilities, in addition to other climate indices. As the AMOC transport results in a net northward transport of heat around 1 PW (10^{15} Watt), it makes a substantial contribution to the mild maritime climate of Northwest Europe and any slowdown in the AMOC would have profound implications for climate in the North Atlantic region. Investigating the link between the AMOC and the SST on decadal timescales, and using coupled climate models, Stouffer et al (2005) found that a hypothetical 100–year shut down in the AMOC would lead to an increased temperature in the southern hemisphere and a decrease of temperature in the northern hemisphere up to 12°C around Greenland and the Nordic Seas.

Since the AMOC transports upper–ocean heat across latitudes, it has been proposed that it may lead to large–scale climate patterns, through the development of SST anomalies (SSTAs) (Robson et al (2012a),Robson et al (2012b)). Results from numerical models suggest that the intra–annual AMOC variability may be rather local and that there is little correlation between the variability found e.g. at 26°N and locations situated a few degrees further north or south (Hirschi et al (2007), Bingham et al (2010)). The implications of a limited meridional coherence of the AMOC on subannual timescales means that there can be anomalous convergence and divergence of heat in the ocean (Cunningham et al (2013), Sonnewald et al (2013), Bryden et al (2014)). An accumulation of heat into a region can result in higher SSTs, and therefore, the AMOC could be an indicator for a developing SSTA. This simple idea is the motivation for us to test whether the available AMOC observations from 26°N can be used to predict the formation of SSTAs.

Since April 2004, an observing system for the AMOC has been deployed and maintained at 26°N in the Atlantic in the framework of the UK–US RAPID–MOCHA project (Hirschi et al (2003), Cunningham et al (2007)). It provides continuous measurements of the strength and vertical structure of the AMOC and its associated heat flux. The decade long time series has provided unexpected insights into the behaviour of the AMOC from seasonal to interannual timescales. One important finding of the RAPID–MOCHA campaign has been that even on intrannual timescales the AMOC exhibits a large temporal variability (Fig. 1). On these timescales, the AMOC variations are caused by both fluctuations in the density field and in the wind stress (Hirschi et al (2007), Chidichimo et al (2010), Kanzow et al (2010), Duchez et al (2014)).

Large fluctuations in the AMOC have also been found on interannual timescales and McCarthy et al (2012) showed a 30% decline in the AMOC for 14 months during 2009–10, where the AMOC transport was 6 Sv weaker in the mean compared to the previous years.

This weak AMOC transport is attributed to an anomalously high southward thermocline transport (where the typical seasonal cycle has vanished) and extreme southward Ekman transports in the winter period. Roberts et al (2013) found that the amplitude of this observed slowdown was extraordinary compared to the simulated AMOC variability and such a weakening was not represented in the variability of a set of 10 CMIP5 coupled climate models. This AMOC event led to a reduced northward ocean heat transport across 26°N by 0.4 PW resulting in colder waters north of 26°N and warmer waters south of 26°N, a spatial pattern that helped push the wintertime atmospheric circulation during both 2009–10 and 2010–11 into record–low negative North Atlantic Oscillation (NAO) conditions associated with severe winter conditions over northwestern Europe (Taws et al (2011), Cunningham et al (2013), Sonnewald et al (2013), Bryden et al (2014), Buchan et al (2014)). In 2010, the warming south of 26°N also coincided with the strongest Atlantic hurricane season since 2005 (Bender et al (2010)).

The 2009–2010 AMOC event is a good example illustrating the main hypothesis of this paper. While the AMOC and Meridional Heat Transport (MHT) reduced at 26°N during this period of time, the MHT did not reduce as much at 41°N (Johns et al (2011), Hobbs and Willis (2013), Bryden et al (2014)). There was thus more heat moving northward through

41°N than coming in at 26°N resulting in an anomalous divergence of heat between these two latitudes. Bryden et al (2014) showed that the SST patterns in winter 2009–2010 conditions were not primarily due to air–sea interactions. Consequently, since volume transport governs heat transport, and the heat transport north of 41°N did not change much, and the surface fluxes did not change enough to explain the cooling, the widespread cooling of the North Atlantic was attributed to the changes in the AMOC at 26°N. The main goal of this paper is to generalise the hypothesis that the AMOC has an influence on the North Atlantic SSTs and assess the link between these two quantities more generally for the 2004–2014 period. We use the first decade (2004–2014) of AMOC observations at 26°N as a precursor of the SST over the North Atlantic region, and aim to determine to what extent knowing the AMOC allows us to predict SSTs. We thus investigate the link between the observed AMOC anomalies at 26°N and satellite based SSTA data (Reynolds et al (2007)), with the AMOC leading the SSTA fluctuations. Section 2 describes the datasets and methods used in this paper. In section 3, we assess the correlation pattern between the AMOC and the North Atlantic SSTAs when the AMOC leads the SSTAs. A discussion and summary of the paper are given in sections 4 and 5, where we further discuss the possible physical mechanisms behind the correlations between AMOC and SSTA when the SSTA leads, alongside hypotheses on the impact of seasonal SST predictions for Atlantic hurricane forecasting and extreme weather in Northwestern Europe.

2 Data and Method

2.1 Data

The data used in this paper cover the period April 2004 – March 2014 and comprise the AMOC observed by the RAPID array at 26°N, satellite based SST data and air–sea fluxes from ERA–Interim (Dee et al (2011)). Monthly data are used throughout and the seasonal cycle is removed from these three datasets.

2.1.1 Calculation of the AMOC by the RAPID array

The AMOC as observed by the RAPID array is defined as the sum of the Gulf Stream through the Straits of Florida (the Florida Straits transport, FST), the meridional Ekman transport (EKM), and an interior transbasin transport estimated from the mooring array. The FST has been monitored using a submarine cable between Florida and the Bahamas using the principles of electromagnetic induction (Baringer and Larsen (2001)) with daily estimates, and repeated ship sections since 1982. The Florida Current cable and section data are made freely available on the Atlantic Oceanographic and Meteorological Laboratory web page (*www.aoml.noaa.gov/phod/floridacurrent/*).

The meridional component of wind–driven Ekman transport is calculated from the zonally–integrated meridional ERA–Interim wind stress across 26°N from the shelf off Abaco (Bahamas) to the African Coast. This transport is applied in the top 100 m.

Finally, the transbasin transport includes a directly estimated component, west of 76.75°W, a geostrophic component east of 76.75°W and a uniform compensation transport, chosen to enforce zero net transport across 26°N (including transbasin, Florida Current and Ekman transports) on a 10–day timescale. This compensation term effectively replaces the choice of a level of no–motion as typically used for transports estimated from hydrographic sections (Roemmich and Wunsch (1985), Bryden et al (2005)). To estimate the geostrophic component of the transbasin transport, the principle of the array is to estimate the zonally integrated geostrophic profile of northward velocity from measurements of temperature and salinity at the eastern and western boundary of the array using the thermal wind relationship.

Overall, the AMOC strength is computed as:

$$AMOC(t) = FST(t) + EKM(t) + UMO(t), \tag{1}$$

where UMO (for Upper Mid–Ocean) is the transbasin transport above the depth of maximum overturning. Data are processed and made available through the RAPID website (*http://www.rapid.ac.uk/rapidmoc*) with a temporal resolution of 12 hours. In the following work, the data obtained from April 2004 to March 2014 were monthly averaged and deseasoned by removing the 12–month climatology obtained from the monthly data. The 12–month climatology is a timeseries defined as the mean of all January data, February data, and so on, up to December. Then, each component (AMOC, FST, EKM and UMO) was de–trended and filtered with a 2–month running mean.

From April 2004 to March 2014, the mean AMOC strength was 17.0 $\pm$ 3.3 Sv (1 Sv=10^6 m^3s^{-1}), FST was 31.4 $\pm$ 2.3 Sv, EKM was 3.6 $\pm$ 2.0 Sv, and the UMO transport was -17.9 $\pm$ 2.7 Sv[1] Full details of the 26°N AMOC calculation can be found in McCarthy et al (2014).

2.1.2 SST Data

SST data are collected from the NOAA optimum interpolation dataset **(NOAA OI, Reynolds et al (2007), *http://www.esrl.noaa.gov/psd/data/gridded/data.noaa.oisst.v2.html*)**. This dataset has a resolution of 1° × 1°, and is based on global satellite observations. SST data were processed the same way as the RAPID data. The data were deseasoned **(and subsequently referred to as** SST anomalies: SSTAs) using the climatology obtained from the monthly SST data from December 1981 to March 2015 **(the longest possible period is used to obtain a robust seasonal cycle)** before being de–trended and filtered. We then extracted the data from April 2003 to March 2015 to span the RAPID era (April 2004 – March 2014). **These**

[1] Positive and negative numbers indicate northward and southward transports, respectively. (the standard deviations mentioned here are based on monthly data after removal of the mean seasonal cycle and the trend).

data were extracted one year before and after the RAPID era in order to perform lagged correlations between the SST data and the AMOC timeseries and components.

2.1.3 Air–Sea heat fluxes

Changes in the local air–sea heat fluxes are a likely contribution to observed SSTA patterns. The heat flux can be divided into four components, the net shortwave and longwave radiation and the sensible and latent heat flux anomalies. Variability in the net shortwave radiation will depend on changes in cloudiness and the sea–ice albedo. Changes in the net longwave radiation are due to changes in the lower atmospheric temperature, cloudiness, or SST. Longwave radiation anomalies tend to damp SSTAs. The sensible and latent heat fluxes depend on gradients between the lower atmosphere and the sea surface in temperature and water vapor pressure respectively. Both latent and sensible heat fluxes depend strongly on the surface wind speed and thus are well correlated.

The air–sea flux (ASF) anomalies used in this paper are extracted from the ERA–Interim reanalysis (Dee et al (2011)) and comprise all four components of the net heat flux (sensible, latent, shortwave and longwave radiations). ERA–Interim is a global atmospheric reanalysis from 1979, continuously updated in real time. The spatial resolution of the data set is approximately 80 km on 60 vertical levels from the surface up to 0.1 hPa. The ERA-Interim data used in this study were downloaded from *http://apps.ecmwf.int/datasets/data/interim-full-daily/*. Analyses using the ERA–Interim ASFs cover the same period April 2004 – March 2014, and the ASF anomalies were calculated by removing the seasonal cycle from 1979 to 2012.

In section 3.3.1, where the role of ASFs on the development of SSTA patterns is assessed, the ERA–Interim SST dataset is used in order to avoid any unnecessary regridding of the Reynolds SST data on the ERA–Interim grid. As the ERA–Interim dataset makes use of satellite data (Dee et al (2011)), it is likely to be close to Reynolds SSTs.

2.2 Method

Unlike previous studies which aimed at predicting the AMOC variability (Hawkins and Sutton (2009), Robson et al (2012a), Robson et al (2014), Sévellec and Fedorov (2014)), we assume in this paper that we know the AMOC, and want to know what we can predict from this starting point.

For this purpose, the RAPID data (the AMOC and components) and the SSTAs were correlated for different time lags. Since our main interest in this paper is to use AMOC information to predict SSTAs, we will mainly focus on situations where the AMOC and its components lead the SSTA fields. These results will be shown in Section 3, while the correlations when SSTAs lead are shown in the discussion section of this paper.

The significance of these correlations is evaluated with a method based on composites. This method consists of generating a thousand random discretised (binary) signals (composites) with similar statistical properties as the RAPID data. For the random selection of months to be statistically comparable to the RAPID AMOC anomaly timeseries we ensure that we randomly pick the same number of months with positive and negative anomalies (i.e. 66 and 54). For example, positive and negative SSTA composites are therefore the averages of 66 and 54 selected months during the 2004–2014 period (Eq. 2 and 3):

$$SSTA^{+} = \frac{\sum_{1}^{N^{+}} SSTA_{t^{+}}}{N^{+}} - \frac{\sum_{1}^{N} SSTA}{N}, \tag{2}$$

$$SSTA^{-} = \frac{\sum_{1}^{N^{-}} SSTA_{t^{-}}}{N^{-}} - \frac{\sum_{1}^{N} SSTA}{N}, \tag{3}$$

where t^+ and t^- are the timings from the positive and negative anomalies in the AMOC (or its components) or from the random sampling mentioned above; N^+ and N^- are the total numbers of positive and negative months and N is the total number of months (N = 120). Therefore, by construction we have:

$$\frac{SSTA^+ \times N^+ + SSTA^- \times N^-}{N} = 0. \tag{4}$$

We ensure that the temporal properties of the random timeseries are comparable to those of the AMOC observations. For this, we compute lagged autocorrelations for discretised transport timeseries (i.e. -1 for AMOC < 0 and 1 for AMOC ≥ 0) and for the equivalent discretised timeseries obtained from the randomly selected timings. For each timeseries the lagged autocorrelations are integrated from lag 0 up to the lag where the first zero–crossing occurs. We only keep the randomly generated timeseries for which the value of the integral is between 0.75 to 1.25 times the value obtained for the RAPID data. We have tested a broader envelope of 0.50–1.50 and our results showed a slightly higher significance for the AMOC–SST correlation. In contrast, narrowing the envelope leads to slightly decreased significance. The range of 0.75–1.25 was found to be a good compromise between allowing too many unrealistic random timeseries or being too strict and not allowing enough freedom for the random timeseries to have enough variety in their temporal properties.

Figure 2 illustrates on top the AMOC with the positive (blue) and negative (red) anomalies, and at the bottom, the SSTA (at a specific location in the North Atlantic) for which $SSTA^+$ and $SSTA^-$ are calculated.

In a last step we use the composite method to determine the statistical significance of the correlations between the RAPID timeseries and SSTA. Absolute composite values (i.e. $abs(SSTA^+)$, $abs(SSTA^-)$) are a measure for the covariance between SST and

the AMOC. For each grid cell the 1000 random composites provide a distribution of values which we compare to the composite value we obtain when using the observed AMOC timeseries. A correlation in a given grid cell is deemed significant if less than 5% of the absolute values (i.e. $abs(SSTA^{+})$, $abs(SSTA^{-})$) found for the randomly generated composites are higher than the values for $abs(SSTA^{+})$ and $abs(SSTA^{-})$ obtained when using the observed RAPID timeseries.

3 Results

The datasets previously described are used in this section in order to test our main hypothesis: the AMOC timeseries can be used to predict the SSTA over the North Atlantic. In this section we therefore concentrate on the case where the AMOC leads SSTAs. The case where SSTAs lead the AMOC is discussed in section 4.

3.1 The North Atlantic SST response to the AMOC variability

To assess the link between the AMOC at 26°N and the SSTA over the North Atlantic, lagged spatial correlations were calculated for lags from zero to 12 months, where the AMOC leads the SSTA. These correlations are shown in Fig. 3 with the AMOC leading the SSTA by 0, 2, 5, 7, 9 and 12 months. The 95% level of significance in these correlations is obtained using the composite method described in Sect. 2.2 and the strongest signal is found when the AMOC leads the SSTA by 5 months (Fig. 3c).

For this specific lag (Fig. 3c), the correlation pattern exhibits a distinct dipole structure where positive correlations are found between the AMOC and the SSTA southeast of Newfoundland between 26 and 45°N and negative correlations occur in a zonal band reaching from the Gulf of Mexico to the African coast between 10 and 26°N. This occurrence of positive/negative can be explained with a simple conceptual model schematised in Fig. 4. As mentioned in the introduction, the meridional coherence of AMOC anomalies on subannual timescales is likely to be small. Therefore, the correlation/anticorrelation pattern in the North Atlantic could be the consequence of a seesaw–like mechanism. A positive AMOC anomaly at 26°N increases the input of oceanic heat into the region north of the RAPID–MOCHA section. At the same time a positive AMOC anomaly extracts more heat from the region south of the RAPID–MOCHA section. An increased input and extraction of heat north and south of the 26°N section is consistent with positive and negative SSTAs north and south of the 26°N section. Conversely, a negative AMOC anomaly is consistent with the development of negative and positive SSTAs north and south of the 26°N section. In order to understand the contribution of each of the AMOC components to the emergence of the SSTA dipole, spatial correlations and composites are also calculated between the SSTA and EKM (Fig. 5b), the FST (Fig. 5c) and the UMO transport (Fig. 5d), the components leading the SSTA. For a lag of 5 months, the EKM component mainly contributes to the development of the tropical part of the dipole while the other components seem to equally contribute to the formation of this SSTA dipole. While a weakening in EKM is associated with a warming of the SSTA off the western European coast (anticorrelation pattern in Fig. 5b), a strengthening in the UMO transport also seems to be associated with a warming in this same area (correlation pattern in Fig. 5d). The 95% significance contours indicate that the FST is the component which contributes the least to the development of this SSTA pattern for this specific lag.

3.2 Spatial and temporal variability of the SSTA over the North Atlantic

3.2.1 Spatial pattern of SST variability

To better characterise the variability of the SST over the North Atlantic, we apply an Empirical Orthogonal Function (EOF) analysis to the North Atlantic SST field from 5° to 80°N and analyse the spatial structure of the dominant mode of variability of SST during the RAPID era (April 2004–March 2014). Details of the EOF methodology can be found in Preisendorfer (1988). Since we do not want our signal to be contaminated by the seasonal warming and cooling of the SST, the annual cycle (calculated from the full SST timeseries available from December 1981 to March 2015) has been removed from our timeseries and the data are first smoothed with a 2–month low pass filter before calculating the EOFs.

The three first EOFs explain almost 40% of the total variance (Fig. 6). The principal component associated with the first EOF shows a large range of variability (up to 2°C) and is characterized by two minima in mid–2005 and mid–2010. The spatial pattern associated with this first mode (Fig. 6b), explains 20.4% of the total variance and is characterized by a distinct tripole structure (also called the North Atlantic SST tripole) that is reminiscent of Atlantic SST patterns discussed in previous studies (e.g. Czaja and Frankignoul (2002), Seager et al (2000), Fan and Schneider (2012)). In this tripole, the tropics (5° to 20°N) and subpolar gyre (50° to 70°N) vary with an opposite sign compared to the subtropical gyre. Buchan et al (2014) and Taws et al (2011) associated this tripole with an exceptionally negative phase of NAO, characterising both cold winters in 2009–2010 and 2010–2011.

Earlier work (Seager et al (2000), Fan and Schneider (2012)) based on the net surface heat flux from the NCEP reanalysis, demonstrated that in the latter half of the 20^{th} century this SST tripole pattern was consistent with being forced primarily by the atmospheric heat flux. Schneider and Fan (2012) examined the role of ocean dynamics and concluded that the influence of the simulated AMOC on the SST tripole was minor. The mechanism explained in the previous section of this paper show that **the AMOC may partially explain** the origin of the subtropical and mid–latitude lobes of the tripole (the 2 patterns at mid and low latitudes) described by this first mode of variability.

The principal component associated with the second mode of variability (explaining 10.1% of the total variance) does not show any particular extreme SSTA value compared to the first mode. The corresponding spatial pattern (Fig. 6c) is also characterised by a tripole pattern which is shifted southward by about 10–15° compared to the first mode, with stronger intensities toward the Nordic Seas and the Atlantic coast of Western Europe as well as an intensified pattern east of Newfoundland.

Finally the principal component associated with the third mode of variability (explaining 8.1% of the variance) shows three maxima, during late 2009, beginning of 2011 and beginning of 2013. The spatial structure associated with this third mode is characterised by a dipole structure north and south of about 30°N but does not resemble the dipole found by relating the AMOC to SSTAs.

3.2.2 Temporal relationship between the AMOC and SSTAs

To further relate the AMOC to the main mode of variability of SSTA over the North Atlantic, we perform cross correlations between the AMOC, its components, and the principal component associated with the first mode of variability of SSTA (Fig. 7). We are interested here in negative lags when the AMOC leads the SSTA. **Some discussion about possible physical mechanisms consistent with the correlations for positive lags will be provided in the discussion section of this paper** (section 4). The strongest correlations between the AMOC and SSTA (the AMOC leading) are reached for lags from 2 to 5 months for which the correlations reach a plateau with values above 0.3, which is in good agreement with the results obtained in Sect. 3.1. For a lag of 3–months for example, the corresponding lagged correlation coefficient is 0.37 (compared to 0.16 without lag) and 0.43 if a 3–month low pass filter is applied to both timeseries. In the following we concentrate on the lag of 5 months as this is the longest lead time that is part of the plateau with increased correlations between AMOC and SSTAs shown in Fig. 7.

Since the observed AMOC is calculated as the sum of EKM, FST and UMO transport, all components contribute to the SSTA anomaly patterns associated with the AMOC (Fig. 5). However, we do not expect the AMOC's components to all contribute at the same time due to the different timescales that govern the physical processes underlying each component (Fig. 7). Between EKM and SSTAs the highest correlation occurs for a lag of 1-2 months. Between FST/UMO and SSTAs the highest correlations are found for lags of 3 and 7 months, respectively.

In summary, during the period 2004–2014, the main mode of SSTA variability is characterised by a tripole pattern over the North Atlantic. **Following the ideas behind the suggested physical mechanism (described in Sect. 3.1) associated with the 2 to 5–month lagged SSTA response to AMOC fluctuations, the AMOC's contribution seems to be limited to the two southern lobes of the SSTA tripole.**

3.3 Is this SSTA dipole a direct response to atmospheric forcing?

Given the small meridional coherence across the 40°N boundary in the AMOC on subannual timescales (Bingham et al (2010), Josey et al (2009)), the main hypothesis in this paper is that the variations in the heat advected by the AMOC at 26°N is not likely to be the same further north resulting in a divergence or convergence of heat between the two latitudes considered and the development of SSTAs. Although the link between the volume transport and heat transport has been established (Sonnewald et al (2013)), as well as the link between the heat transport and heat content in the ocean, a change in the heat content is not necessarily accompanied by a change in the SST. Ocean heat content changes may remain confined to the subsurface and SSTAs can directly result from air-sea fluxes.

Changes in ocean temperatures are partly due to radiative and turbulent heat exchanges at the air–sea interface, and due to advective heat transport divergence resulting from varying ocean currents (Bjerknes (1964)). To make sure that the heat advected by the AMOC is responsible for the SSTA dipole structure previously described, we need to make sure that these SSTA fluctuations are not just the response to atmospheric heat fluxes.

3.3.1 Air–Sea fluxes

To determine the areas where the SSTA variance is more likely to be explained by air–sea exchanges, spatial correlations between the cumulated air–sea flux (ASF) anomalies and SSTAs are calculated over the North Atlantic (Fig. 8), where ASFs lead SSTAs.

A positive correlation indicates that both the ASF anomalies and SSTAs vary with the same sign. This can occur if positive ASF anomalies (which imply either that more heat is gained by the ocean or less heat is lost) tend to be co-located with positive SSTAs (or vice versa i.e. negative heat flux anomalies with negative SSTAs). In each case, the SSTA is consistent with an ocean response to atmospheric forcing e.g. more heat gain by the ocean leads to surface warming. Positive correlations thus indicate the areas where the SSTAs can be seen to be a response to the ASF anomalies as opposed to being their source. In the latter case a negative correlation would be expected as for example positive SSTAs are now associated with negative air–sea heat flux anomalies i.e. increased ocean heat loss or less heat gain.

In order to compute these correlations, the SSTA timeseries has been correlated to the ASF anomaly timeseries cumulated over an increasing number of months from 2 months (Fig. 8b) to 12 months (Fig. 8l). If we focus on the area where the AMOC–SSTA dipole was located (shown in Fig. 5a), positive correlations mainly occur in a band reaching from 12°N to 26°N, the strength of this correlation increasing with increasing accumulation of months in the ASF data. In this band of latitudes, maximum correlations occur around 6–7 months and explain up to 25% of the SSTA variance. This means that for shorter periods of time between 2 and 5 months when we showed highest correlations between the AMOC and the SSTA in the dipole previously described, the SSTA is not mainly responding to a forcing from atmospheric heat fluxes and ASFs contribute to a lesser extent to the development of this SSTA dipole (explaining less than 16% of the variance around the lower lobe of the dipole).

In summary, the strongest correlations between the cumulative ASFs and SSTAs are found at lags from 6 to 7 months and over most of the North Atlantic, these correlations are lower than 0.3 (e.g. the region coinciding with the northern lobe of the SSTA dipole of Fig. 5). For lags between 2 and 5 months when the AMOC/SSTA correlations are the strongest, the ASF/SSTA correlations are even lower.

3.3.2 Ekman transport

Second to the surface heat flux, the most effective driver of SST variations is the wind–induced Ekman heat transport, especially along oceanic thermal fronts, such as the Gulf Stream (Frankignoul (1985)). Lagged correlations and composites between EKM and the SSTA are shown in Fig. 9 at zero lag (Fig. 9a), for a lag of 2 months (Fig. 9b), 5 months (Fig. 9c), 7 months (Fig. 9d), 9 months (Fig. 9e) and 12 months (Fig. 9f), EKM leading the SSTA. **The strong correlations found south of about 40°N for lags of up to 2 months**

indicate that EKM plays a significant role in setting the SSTA response pattern up to this latitude, but can only partly explain the dipole structure shown in Fig. 5a. At a lag of 5 months, EKM explains the tropical lobe of the dipole but for the northern lobe, significant correlations are only found in the eastern part of the basin. Generally, the correlation between EKM and the SSTA decreases as the lag increases beyond lags of two months.

To further assess the contribution of EKM to the link previously made between the AMOC and the SSTA, the EKM component has been subtracted from the AMOC (called "AMOC–EKM", Fig. 10b and d, Mielke et al (2013)) before calculating the correlations between the AMOC and the SSTA. At zero lag (Fig. 10a and b), the correlations between the AMOC and SSTA and AMOC–EKM and SSTA show different spatial patterns, highlighting the role previously demonstrated of EKM in the characterisation of this pattern. For a lag of 5 months (Fig. 10c and d), these spatial correlations show a very similar spatial structure; the main difference between these figures being the intensity of the negative correlation between 0 and 20°N. This indicates that for these longer periods of time, EKM is predominantly contributing to the development of the southern part of the SSTA tripole.

4 Discussion

That the Atlantic has a large impact on the climate of northwestern Europe is an old concept (e.g. Maury (1855)). The prominent mode of Atlantic variability, the Atlantic Multidecadal Oscillation (AMO: the averaged SST over the whole North Atlantic) has been linked with rainfall in the Sahel, India and northwest Brazil, hurricane formation in the Atlantic and northern hemisphere mean temperature fluctuations (Knight et al (2006), Zhang and Delworth (2006)). In terms of the impact on northwestern Europe, positive AMO leads to warmer temperatures and wetter summers (e.g. Sutton and Dong (2012)). Several modelling studies have shown a relationship between the AMOC and the AMO at decadal and longer timescales (Griffies and Bryan (1992), Latif et al (2004), Knight et al (2006)). Still at decadal timescales, the AMO has recently been shown to be preceded by changes in the North Atlantic ocean circulation (McCarthy et al (2015)). In this study, we show for the first time the potential of the AMOC timeseries at 26°N to be used to predict the Atlantic SST at seasonal timescales.

We show in this paper that the SSTA response to the AMOC variability at a maximum lag of 5 months is characterised by a dipole with a tropical and a subtropical lobe (Fig. 3). The tropical pattern covers the latitudes from 5 to 26°N and thus includes the Main Development Region (MDR) for hurricane formation: 10–20°N, 30–60°W. The benefit of having estimates of Atlantic SST patterns half a year in advance is that SSTAs could then be linked to an increased or decreased probability of storm formation. Due to its potential for widespread destruction, hurricane activity is a noteworthy feature of interannual climate variability, deserving of further investigation into the contributing large–scale processes and associated predictability. Statistical analyses have shown that Atlantic basin hurricane counts depend on Atlantic SST on interannual and longer timescales and that tropical Atlantic SST accounts for a third of interannual hurricane count variability (Elsner et al (2008), Saunders and Lea (2008)). It is also not understood exactly how warm SSTs influence tropical cyclone formation, though it is likely through sustained vertical motion, convective processes and cloudiness.

The MDR for hurricanes, 10–20°N, 30–60°W, has been anomalously warm since 1995 and tropical cyclone activity has also been above average since then. 2005 and 2010 had record high SSTs in the MDR (which is well illustrated in the principal component of the first mode of SSTA over the North Atlantic: Fig. 6a), and correspondingly significant devastating major hurricane landfall activity (Trenberth and Shea (2006)).

The link established in this paper between the AMOC and the SSTA over the North Atlantic region suggests that estimating the AMOC transport could provide some additional information for statistical and dynamical tropical cyclone forecast models by improving SST forecasts for the following season (e.g., LaRow et al (2010), Vecchi et al (2011), Davis et al (2015), Camp et al (2015)). Indeed, conditions may be more conducive than usual to tropical cyclone development when subtropical AMOC transport is anomalously low and heat builds up south of 26°N. The lead time of 5 months between the AMOC and the SSTA would be important for forecasting climate conditions in advance in order to make preparations.

In addition to the relationship demonstrated in this paper, showing that the AMOC (and components) leads an SSTA dipole by up to 5 months, Fig. 7 also suggests an interesting link between SSTAs and the AMOC and components when the SSTA leads. Focusing on lags when the SSTA leads, a correlation of -0.32 is found between the AMOC and SSTA when a lag of 7 months is applied to the SSTA (the SSTA leading), this correlation increasing to -0.43 when a 3–month low–pass filter is applied to the data (Fig. 7). The lagged correlations between the first mode of SSTA variability and the AMOC components (Fig. 7) show that UMO is the main contributor to the correlation pattern between the AMOC and SSTAs. EKM and FST only provide a minor contribution. The spatial correlation patterns between SSTAs and the AMOC (Fig. 11) confirm that the maximum correlation is reached for a lag around 7 months, characterised by a tripole SSTA pattern with significant positive correlations between 0 and about 25°N and 45 to 60°N and a band of significant negative correlations in between. This correlation pattern gradually increases up to 7 months and decreases afterwards. Fig. 12 confirms the weak link found between the SSTA and EKM when the SSTA leads the correlation. Maximum correlations are also found for a lag of 7 months with significant correlation patterns constrained to the central part of the basin between 25 and 45°N.

The lagged correlations between SSTAs and the UMO transport (Fig. 13) show the tripole pattern described for the SSTA/AMOC correlations with significant correlations from lag 1 up to lag 7 when it reaches its maximum. A positive UMO (AMOC) anomaly is then preceded by positive SSTAs at low latitudes (with a 7–month lag). The high correlations originate 7 months in advance in the lower lobe of the tripole south of about 30°N when the correlation is maximal (Fig. 13d).

Focusing on the eastern part of the basin (African coast) the area of positive correlations then propagates northward along the coast up to the Spanish coast at a lag of 1 month. For lags from 3 to 1 month (Fig. 13a–b)) a narrow area of significant correlations extends northwards past the Canaries and covers the latitudes around the 26°N section where the RAPID moorings used to compute the UMO transport are located. This band of positive correlation could possibly be associated with Kelvin (or more generally boundary trapped) waves.

In order to better understand the physical mechanisms explaining the link between the SSTA and UMO transport when the SSTA leads, a closer look to the thermal wind relationship is needed (Eq. 5):

$$v_{geo}(z) = -\frac{g}{\rho f L}\int_{bottom}^{z} (\rho_e - \rho_w)\, dz. \tag{5}$$

This equation computes the mid–ocean geostrophic velocities used to estimate the UMO transport, and L is the basin width, f is the Coriolis parameter, g is the acceleration of gravity, ρ is the density of sea water and ρ_w and ρ_e are the densities at the western and eastern boundary of the 26°N section respectively. From Eq. 5, we can see that if the eastern boundary of 26°N is warmer than usual (around 26°N: Fig. 13a–b), assuming a constant salinity, we expect a smaller density at the eastern boundary and a smaller difference between the density at the eastern and western boundary of the array, which would lead to a weaker (southward) UMO transport (i.e. v_{geo} becomes less negative). For example, a SSTA of +1°C (warmer at the eastern boundary, and if we assume a vertical extent of this anomaly of 200m) would correspond to a density anomaly of approximately 0.25 kg/m^3, leading to an anomaly in the UMO transport of 1.5 Sv, which is of similar magnitude compared to the standard deviation of 2.7 Sv previously mentioned.

Consequently, the propagating correlation pattern seen in Fig. 13a–b around 26°N suggests the development of a positive temperature anomaly that leads to a decrease of the UMO transport and to an increase of the AMOC. This is consistent with a positive correlation between SSTAs and the UMO transport (Fig. 13) and SSTAs and the AMOC (Fig. 11), in the lower lobe of the tripole.

Of course SSTA patterns can be deceptive and we would need to know the vertical density structure to be sure that the SSTAs are indeed consistent with a strengthening of the geostrophic transport. The analyses presented in this paper are based on a joint use of observation–based products, which allowed us to test our hypotheses on 10 years of data. Using a 1/4° NEMO simulation, Grist et al (2010) partitioned annual-timescale ocean heat content anomalies between surface fluxes and ocean heat transport, finding that ocean heat transport (divergence) dominates interannual variability of ocean heat content (and probably SST) in extratropics, while both contribute in similar measure in the tropics/sub–tropics. Future work will consist in reproducing the analyses performed in this paper using high–resolution coupled climate model output (not yet available) in order to check the validity of our results using longer timeseries. Using high–resolution coupled models will be crucial in order to test the impact of the coupling (and hence the representation of air–sea interactions) on our results.

5 Summary and Conclusions

We have tested the potential of the AMOC observations from 26°N between April 2004 and March 2014 to be used to predict SSTs. Our results suggest that:

- There is a significant link between AMOC anomalies and SSTAs where the AMOC leads SSTAs by lags between 2 and 5 months. For positive (negative) AMOC anomalies the SSTA pattern consists of a dipole with negative (positive) SSTAs in the tropical Atlantic and positive (negative) SSTAs to the southeast of Newfoundland.
- All AMOC components contribute to the SSTA pattern found at a 5–month lag. The southern part of the dipole can mainly be linked to the Ekman component, whereas UMO, Ekman and to a lesser extent FST contribute to the northern part of the dipole.
- The SSTA dipole found at a lag of 5 months cannot be attributed to the action of instantaneous air–sea fluxes. Cumulative air–sea fluxes mainly explain the SSTA fluctuations for lags longer than 6–7 months and only explain a small fraction of the SSTA variability for lags from 2 to 5 months when the AMOC/SSTA correlations are the strongest.
- The southern part of the SSTA dipole found at a lag of 5 months encompasses the MDR for Atlantic hurricanes. Our results therefore suggest a potential use of AMOC observations from 26°N to be used to complement existing seasonal hurricane forecasts in the Atlantic.
- Investigating the link between the SSTA and AMOC and its components when the SSTA leads the transport anomalies, a significant relationship was found between the SSTA and the AMOC for a lag of 7 months. This correlation is mainly attributed to the UMO

transport where anomalously high temperatures at the eastern boundary of 26°N for lags between 0 and 3 months are consistent with a reduced southward UMO transport and an increased AMOC.

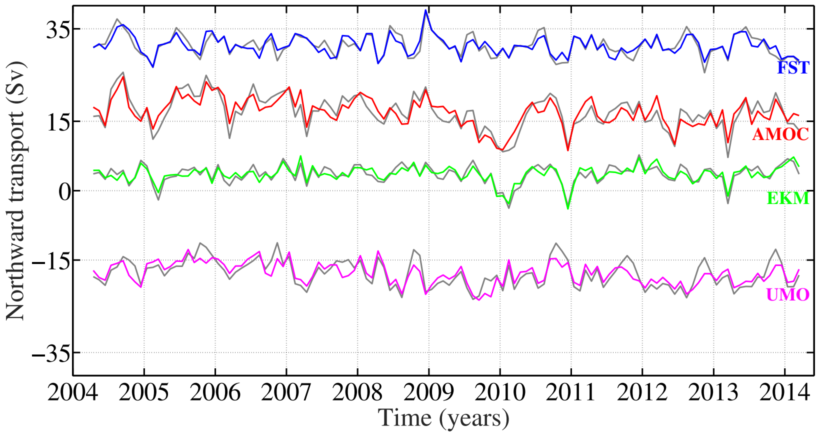

Fig. 1 Timeseries of the AMOC anomaly and the anomaly of its components (the seasonal cycle is removed in coloured plots) measured by the RAPID array at 26°N from April 2004 to March 2014 (monthly mean data). The Florida Straits transport (FST) is derived from electromagnetic cable measurements in the Florida Straits and is represented in blue. The Ekman transport (EKM) is derived from ERA–Interim wind estimates and is represented in green. The Upper Mid–Ocean (UMO) transport is derived from geostrophic velocity profiles from moored instruments across the Atlantic Ocean and is represented in pink. The AMOC transport is the sum of the FST, EKM and UMO transports and is shown in red. Grey curves show the same timeseries with the monthly seasonal cycle included.

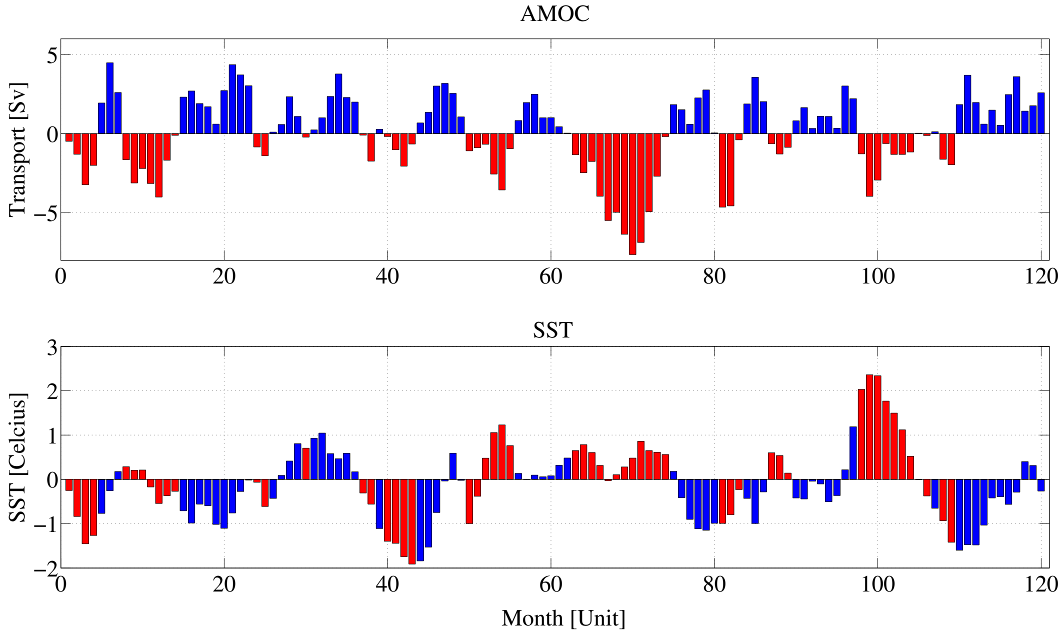

Fig. 2 Bar plot of the AMOC anomaly timeseries with 66 positive values in blue and 54 negative ones in red (top panel). The bottom figure shows the SST anomaly (SSTA) at a specific location (9.5°N, 80.5°W) where the SSTAs in red and blue correspond to the AMOC negative and positive values, respectively.

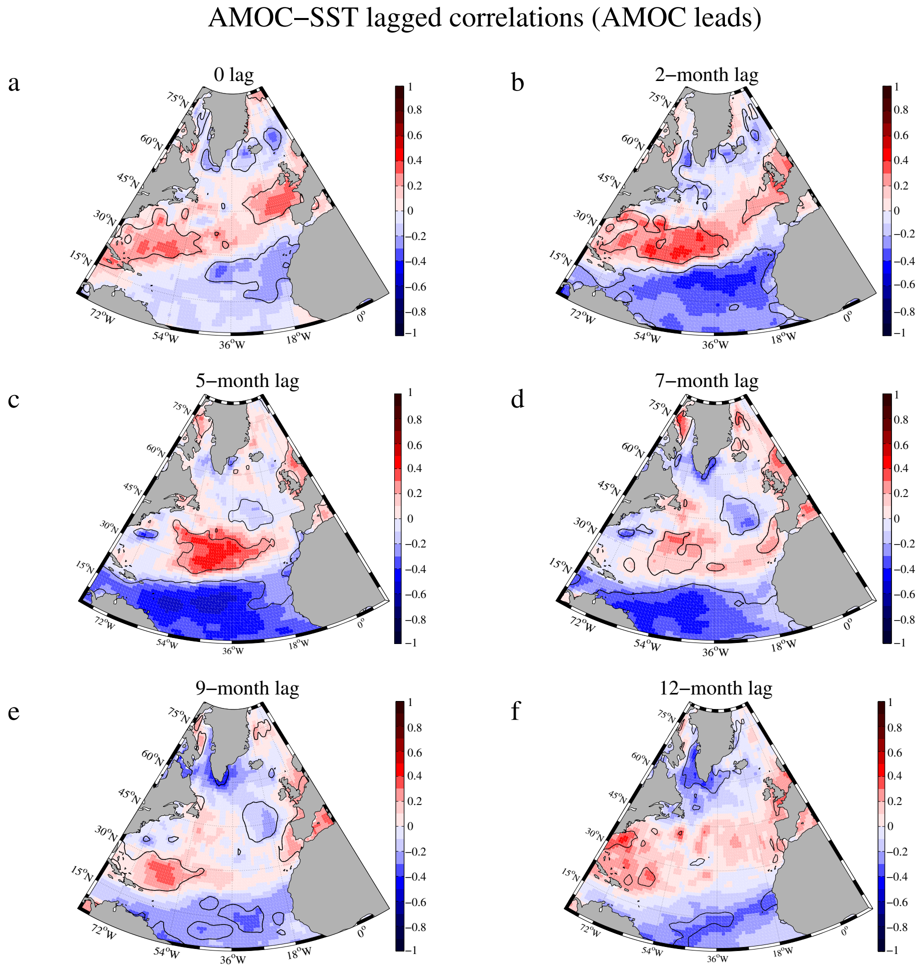

Fig. 3 Lagged correlations between the SSTA over the North Atlantic and the AMOC at 26°N. In these correlations, the AMOC leads the SSTA. Panel (a) shows zero lag, panel (b) shows a lag of 2 months, panel (c) 5 months, panel (d) 7 months, panel (e) 9 months and panel (f) 12 months. Black contours indicate 95% significance levels and were obtained using the composite method.

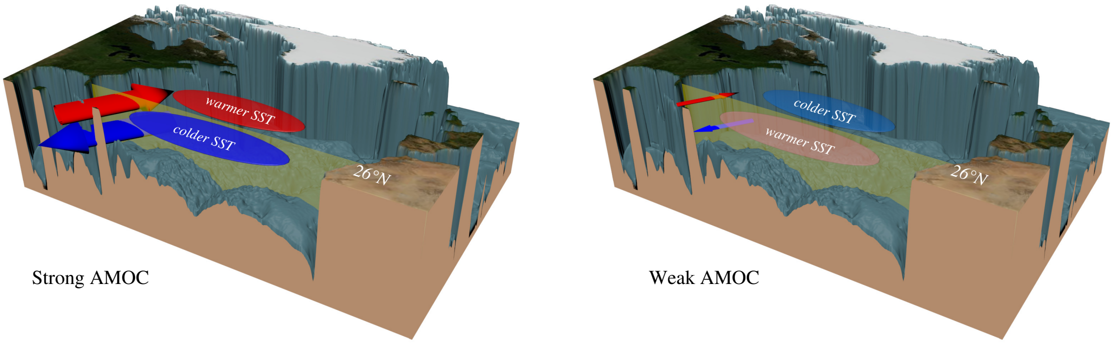

Fig. 4 Schematics representing a seesaw mechanism relating the AMOC fluctuations (upper red and lower blue arrows) to the SSTA pattern (red and blue patches at the surface) in the North Atlantic. The 26°N section is represented by a yellow wall on this figure. A stronger AMOC advects more heat north of 26°N and leads to warmer subtropics and colder tropics as more heat is extracted from this region.

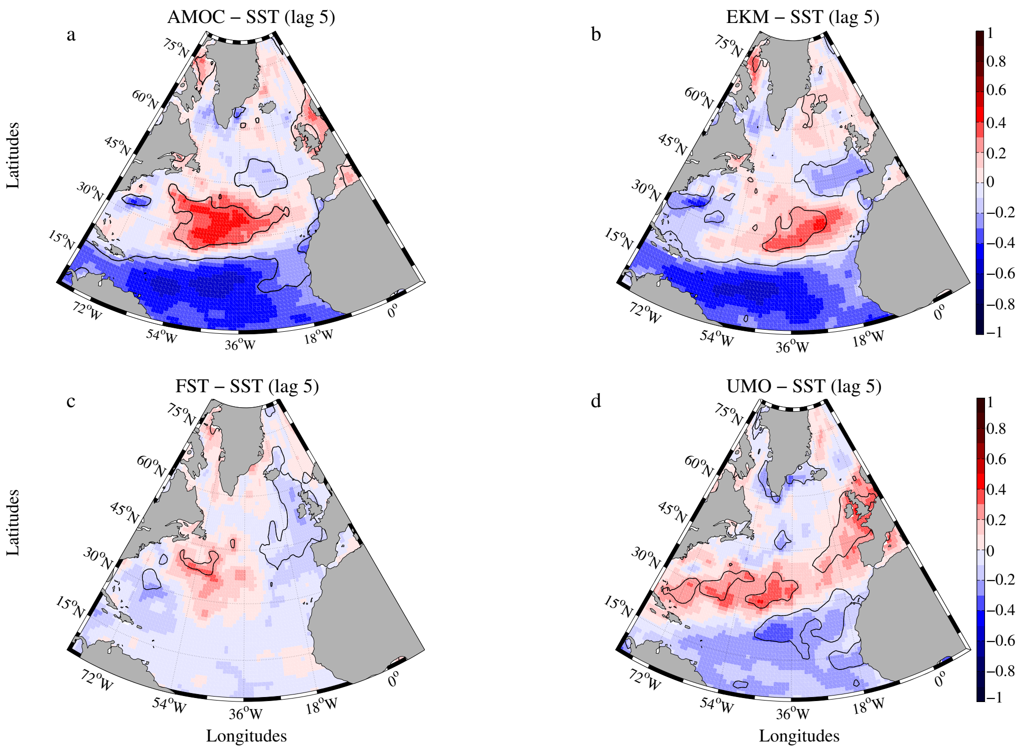

Fig. 5 Correlation between the SSTA over the North Atlantic and the AMOC (panel a, same as Fig. 3c), the Ekman transport (panel b), the Florida Straits transport (panel c) and the Upper Mid–Ocean transport (panel d) at 26°N. Black contours indicate 95% significance levels and were obtained using the composite method. For these figures, the AMOC and components lead the SSTA.

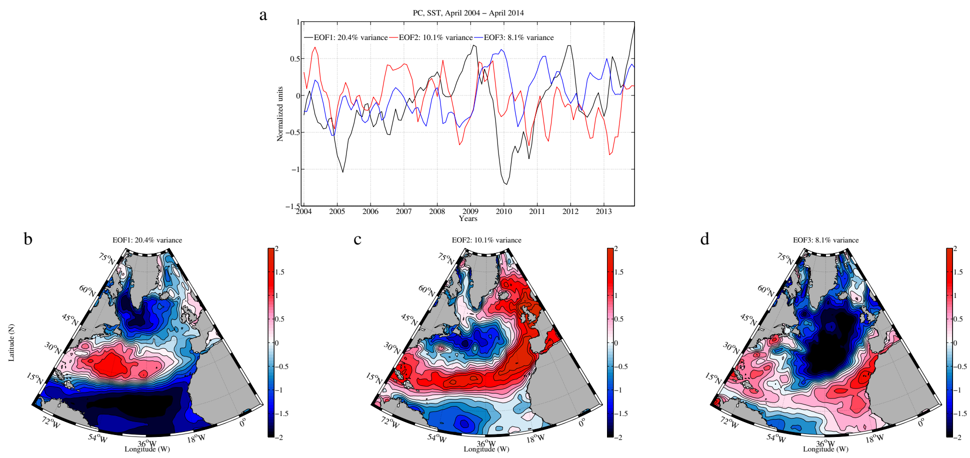

Fig. 6 Conventional Empirical Orthogonal Function (EOF) analysis of SSTA over the North Atlantic. Panel (a) shows the principal components associated with the 3 first EOFs, panel (b) shows the spatial pattern associated with the first mode of variability, panel (c) with the second mode and panel (d) with the third mode.

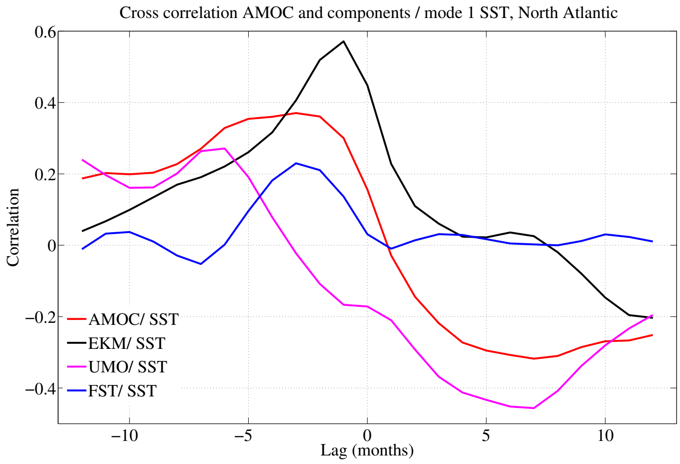

Fig. 7 Cross correlations between the principal component associated with the first mode of variability of SSTA over the North Atlantic and the AMOC (red), the Ekman transport (black), the Upper Mid–Ocean transport (pink) and the Florida Straits transport (blue). Negative lags show correlations when the AMOC and components lead the SSTA. When the AMOC and components lead, the maximum correlations are obtained for a lag between 2 and 5 months for the AMOC, 1 month for the Ekman transport, 7 months for the Upper Mid–Ocean transport and 3 months for the Florida Straits transport. When the SSTA leads, the maximum correlation between the AMOC and SSTA is reached for a lag of 7 months, similar to the UMO transport.

Correlations, cumulative ASF / SST (ASF leads)

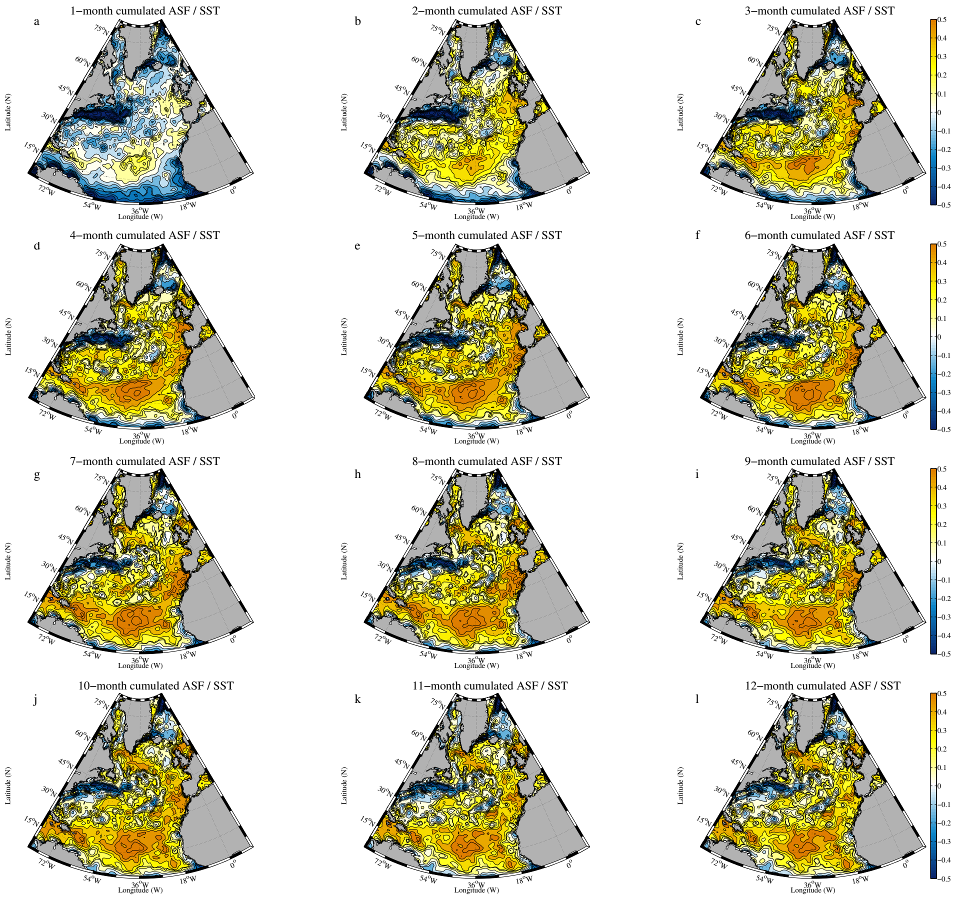

Fig. 8 Correlations between the cumulative air–sea flux anomalies and the SSTAs. For each panel of this figure, we test the time-related impact of the air–sea fluxes on the SSTA. For panel a, instantaneous air–sea fluxes are correlated to the SSTA. For panel b, 2–month accumulated air–sea fluxes are correlated to the SSTA and so on for an accumulation between 2 months (panel) and 12 months (panel l). Thick black lines show the 95% significance level.

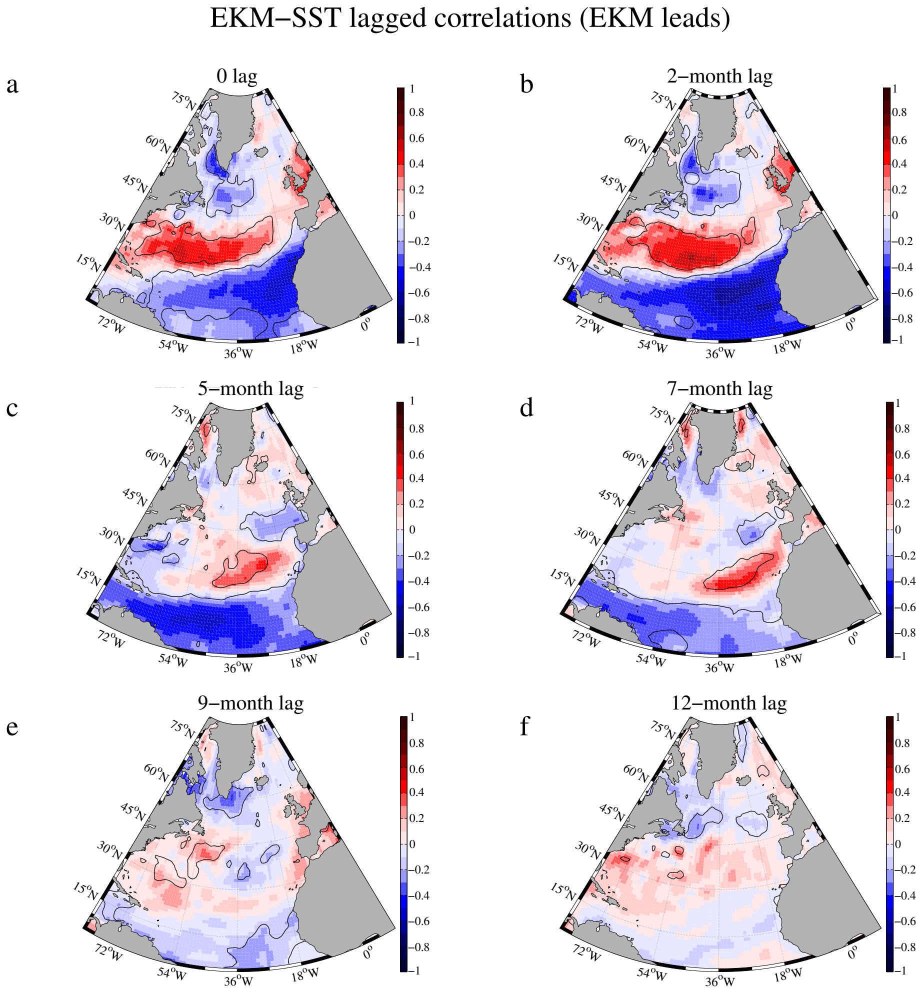

Fig. 9 Lagged correlations between the SSTA over the North Atlantic and the Ekman transport at 26°N. In these correlations, the Ekman transport leads the SSTA. Panel (a) shows zero lag, panel (b) shows a lag of 2 months, panel (c) 5 months (same as Fig. 5b), panel (d) 7 months, panel (e) 9 months and panel (f) 12 months. Black contours indicate 95% significance levels and were obtained using the composite method.

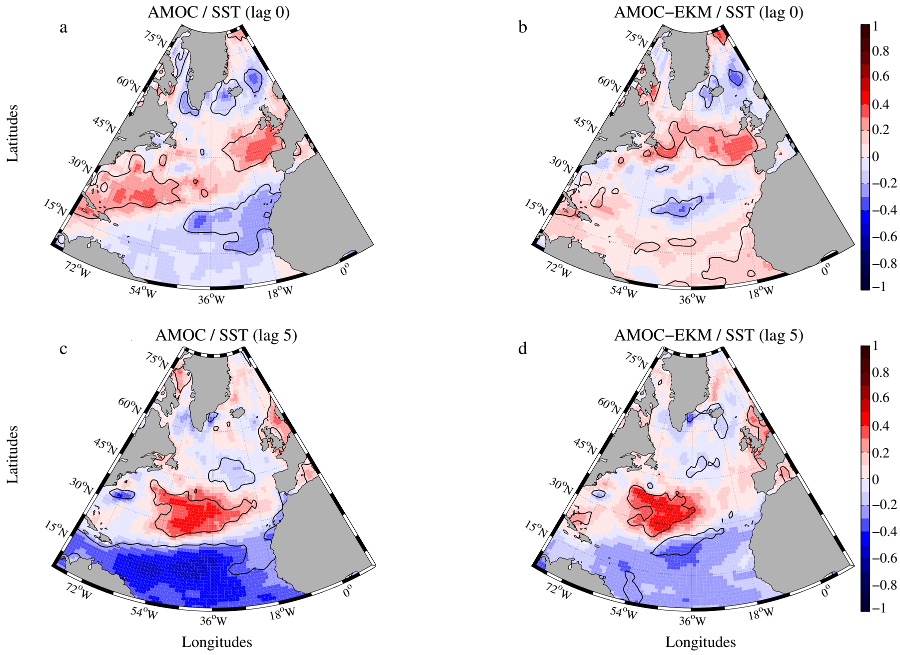

Fig. 10 Spatial correlation between the AMOC at 26°N and the SSTA over the RAPID period (April 2004 – March 2014) at zero lag (panels a and b) and 5–month lag (panels c and d). Panels (a) and (c) show the AMOC while the Ekman component has been subtracted to the AMOC in panels (b) and (d). Note that panels (a) and (c) are similar to panels (a) and (c) in Figure 3.

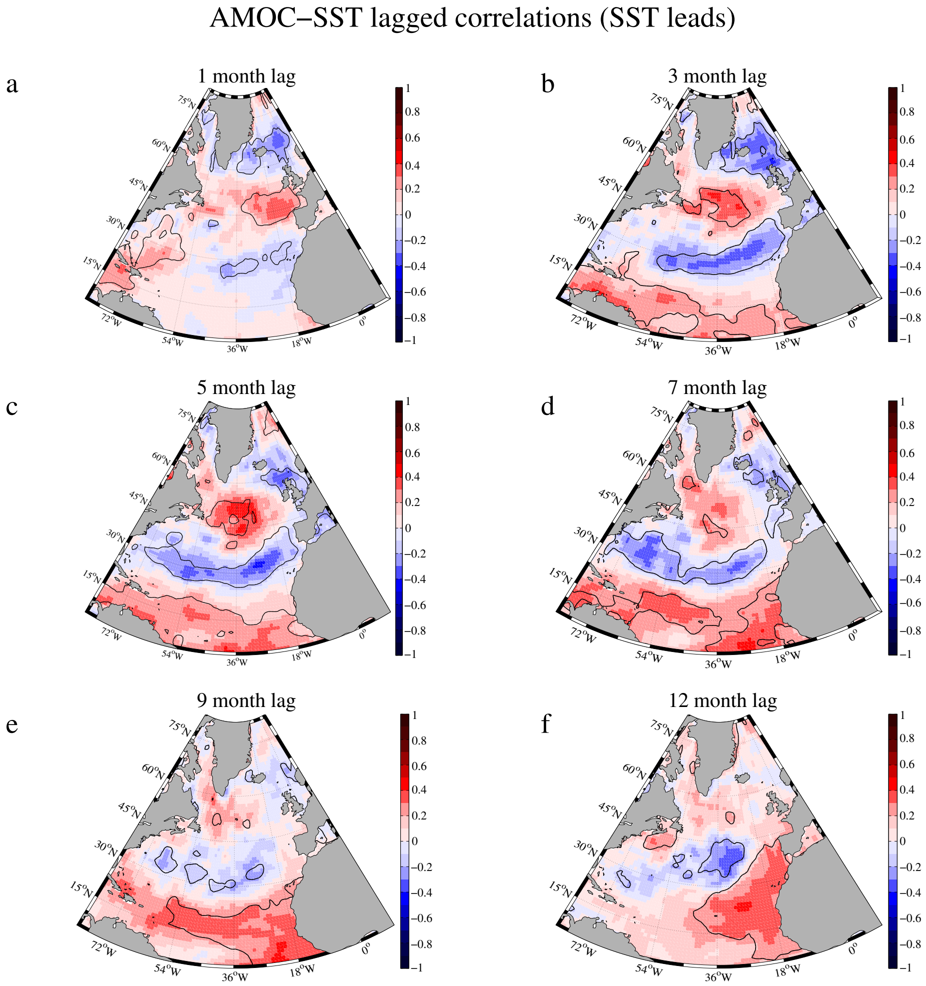

Fig. 11 Lagged correlations between the SSTA over the North Atlantic and the AMOC at 26°N. In these correlations, the SSTA leads the AMOC. Panel (a) shows zero lag, panel (b) shows a lag of 2 months, panel (c) 5 months, panel (d) 7 months, panel (e) 9 months and panel (f) 12 months. Black contours indicate 95% significance levels and were obtained using the composite method.

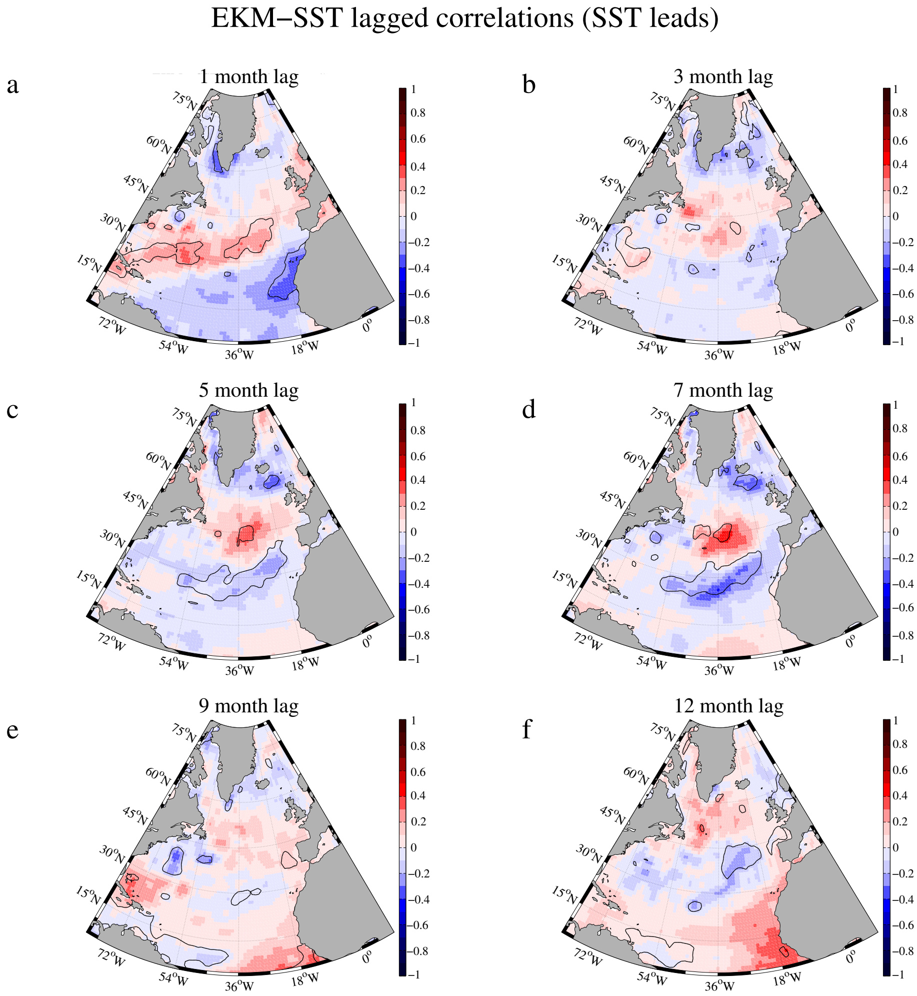

Fig. 12 Lagged correlations between the SSTA over the North Atlantic and the Ekman transport at 26°N. In these correlations, the SSTA transport leads the Ekman transport. Panel (a) shows zero lag, panel (b) shows a lag of 2 months, panel (c) 5 months (same as Fig. 5b), panel (d) 7 months, panel (e) 9 months and panel (f) 12 months. Black contours indicate 95% significance levels and were obtained using the composite method.

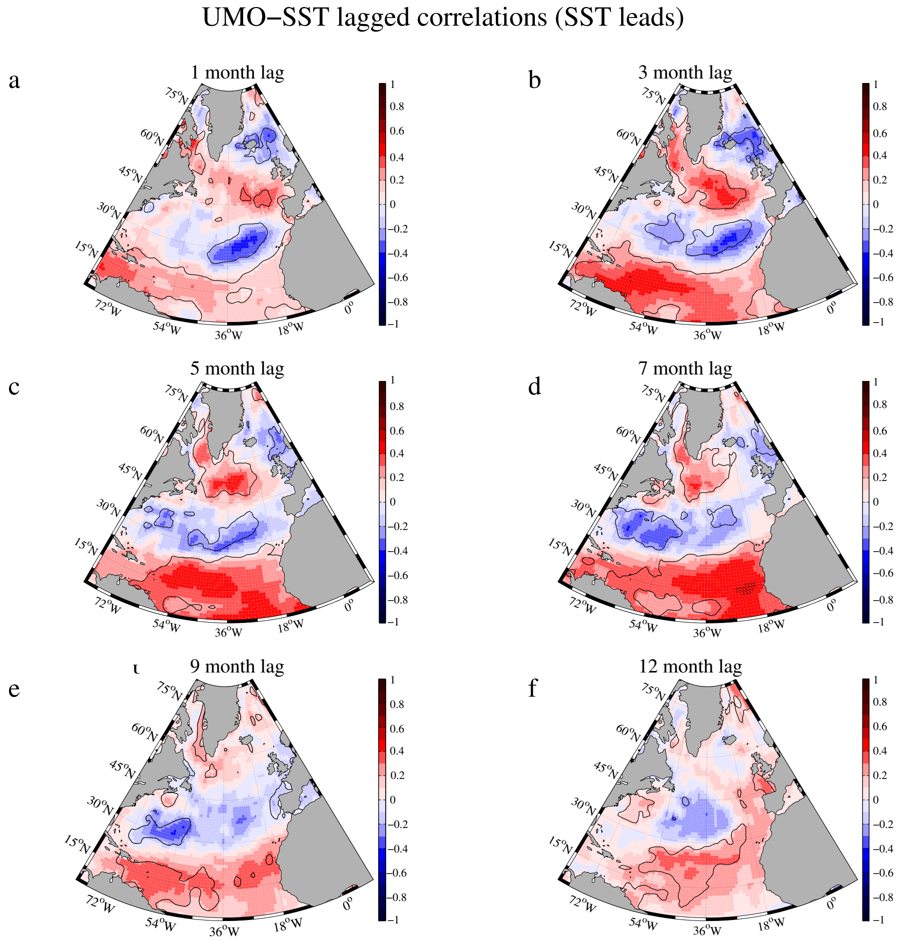

Fig. 13 Lagged correlations between the SSTA over the North Atlantic and the UMO transport at 26°N. In these correlations, the SSTA leads the UMO transport. Panel (a) shows zero lag, panel (b) shows a lag of 2 months, panel (c) 5 months (same as Fig. 5b), panel (d) 7 months, panel (e) 9 months and panel (f) 12 months. Black contours indicate 95% significance levels and were obtained using the composite method.

Acknowledgements Data from the RAPID–WATCH/MOCHA project are funded by the Natural Environment Research Council (NERC) and National Science Foundation (NSF) and are freely available from www.noc.soton.ac.uk/rapidmoc. A. Duchez is supported by the AXA Research fund and NERC. The authors would like to thank Eleanor Frajka–Williams, Harry Bryden and Gerard McCarthy for helpful discussions as well as Clément Fontana for Figure 4. We also thank the two anonymous reviewers and the editor for their thoughtful comments that significantly helped to improve the manuscript. The authors declare that they have no conflict of interest.

References

Baringer MO, Larsen J (2001) Sixteen years of Florida Current transport at 27°N. Geophys Res Lett 28:31793182

Bender MA, Knutson TR, Tuleya RE, Sirutis JJ, Vecchi GA, Garner ST, Held IM (2010) Modeled impact of anthropogenic warming on the frequency of intense Atlantic hurricanes. Science 327:454–458

Bindoff NL, Willebrand J, Artale V, Cazenave A, Gregory JM, Gulev S, Hanawa K, Qur CL, Levitus S, Nojiri Y, Talley CKSLD, Unnikrishnan AS (2007) Observations: Oceanic Climate Change and Sea Level. In: Climate Change 2007: The Physical Science Basis. Cambridge University Press, pp. 385-432. ISBN 0521705967

Bingham RJ, Hughes CW, Roussenov V, Williams RG (2010) Meridional coherence of the North Atlantic meridional overturning circulation. Geophys Res Letter 34:L23,606, doi:10.1029/2007GL031,731

Bjerknes J (1964) Atlantic air-sea interaction. Geophysics (eds H E Landsberg and J Van Mieghem), Academic Press, New York 182:1–82

Bryden H, Longworth HR, Cunningham SA (2005) Slowing of the Atlantic meridional overturning circulation at 25°N. Nature 438 (7068):655–657

Bryden H, King BA, McCarthy GD, McDonagh EL (2014) Impact of a 30% reduction in Atlantic meridional overturning during 2009–2010. Ocean Sci Discuss 11:789–810

Buchan J, Hirschi JJM, Blaker A, Sinha B (2014) North Atlantic SST Anomalies and the Cold North European Weather Events of Winter 2009/10 and December 2010. Monthly Weater Review 142:922–932

Camp J, Roberts M, MacLachlan C, Wallace E, Hermanson L, A Brookshaw A, Scaife AA (2015) Seasonal forecasting of tropical storms using the Met Office GloSea5 seasonal forecast system. J R Meteorol Soc DOI:10.1002/qj.2516

Chidichimo MP, Kanzow T, Cunningham SA, Marotzke J (2010) The contribution of eastern-boundary density variations to the Atlantic meridional overturning circulation at 26.5°N. Ocean Sci 6:475–490

Collins M, Sinha B (2003) Predictability of decadal variations in the thermohaline circulation and climate. Geophys Res Lett 30(6):1–4

Cunningham SA, Kanzow T, Rayner D, Baringer MO, Johns WE, Marotzke J, Longworth HR, Grant EM, Hirschi JJM, Beal LM, Meinen CS, Bryden HL (2007) Temporal variability of the Atlantic Meridional Overturning Circulation at 26°N. Science 317:935–938

Cunningham SA, Roberts CD, Frajka-Williams E, Johns WE, Hobbs W, Palmer MD, Rayner D, Smeed DA, McCarthy G (2013) Atlantic Meridional Overturning Circulation slowdown cooled the subtropical ocean. Geophys Res Lett 40:6202–6207

Czaja A, Frankignoul C (2002) Observed Impact of Atlantic SST Anomalies on the North Atlantic Oscillation. J Climate 15:606–623

Davis K, Zeng X, Ritchie EA (2015) A New Statistical Model for Predicting Seasonal North Atlantic Hurricane Activity. Wea Forecasting 30:730–741

Dee DP, Uppala SM, Simmons AJ, Berrisford P, Poli P, Kobayashi S, Andrae U, Balmaseda MA, Balsamo G, Bauer P, Bechtold P, Beljaars ACM, van de Berg L, Bidlot J, Bormann

N, Delsol C, Dragani R, Fuentes M, Geer AJ, Haimberger L, Healy SB, Hersbach H, Holm EV, Isaksen L, Kallberg P, Kohler M, Matricardi M, McNally AP, Monge-Sanz BM, Morcrette JJ, Park BK, Peubey C, de Rosnay P, Tavolato C, Thepaut JN, Vitart F (2011) The ERA-Interim reanalysis: configuration and performance of the data assimilation system. Quart J Roy Meteor Soc 137:553–597

Duchez A, Frajka-Williams E, Castro N, Hirschi J, Coward A (2014) Seasonal to interannual variability in density around the canary islands and their influence on the Atlantic Meridional Overturning Circulation at 26°N. J Geophys Res Oceans 119:1843–1860

Elsner JB, Jagger TH, Dickinson M, Rowe D (2008) Improving Multiseason Forecasts of North Atlantic Hurricane Activity. Journal of Climate 21:12091219

Emanuel K (2005) Increasing destructiveness of tropical cyclones over the past 30 years. Nature 436:doi:10.1038/nature03,906

Fan M, Schneider EK (2012) Observed Decadal North Atlantic Tripole SST Variability. Part I: Weather Noise Forcing and Coupled Response. J Atmos Sci 69:35–50

Frankignoul C (1985) Sea Surface Temperature Anomalies, Planetary Waves, and Air-Sea Feedback in the Middle Latitudes. REVIEWS OF GEOPHYSICS 23 (4):357–390

Ganachaud A, Wunsch C (2002) Large-scale ocean heat and freshwater transports during the World Ocean Circulation Experiment. Journal of Climate 16:696–705

Goldenberg SB, Landsea CW, Mestas-Nunez AM, Gray WM (2001) The recent increase in atlantic hurricane activity: Causes and implications. Science 293:474–479

Gordon AL, Zebiak SE, Bryan K (1992) Climate variability and the Atlantic Ocean. Eos Trans AGU: 73:161–165

Griffies SM, Bryan K (1992) Predictability of North Atlantic Multidecadal Climate Variability. Science 275:181–184

Grist JP, Josey SA, Marsh R, Good SA, Coward AC, de Cuevas BA, Alderson SG, New AL, Madec G (2010) The roles of surface heat flux and ocean heat transport convergence in determining Atlantic Ocean temperature variability. Ocean Dynamics 60(4):771–790

Hawkins E, Sutton R (2009) Decadal Predictability of the Atlantic Ocean in a coupled GCM: Forecast skill and optimal perturbations using linear inverse modeling. J Climate 22:3960–3978, doi: http://dx.doi.org/10.1175/2009JCLI2720.1

Herweijer C, Seager R, Winton M, Clement A (2005) Why the ocean heat tranport warms the global mean climate? Tellus 57A:662–675

Hirschi JJM, Baehr J, Marotzke J, Stark J, Cunningham SA, Beismann JO (2003) A monitoring design for the Atlantic Meridional Overturning Circulation. Geophys Res Lett 307:doi:10.1029/2002GL016,776

Hirschi JJM, Killworth P, Blundell J (2007) Subannual, seasonal and interannual variability of the North Atlantic meridional overturning circulation. J Phys Oceanogr 37:1246–1265

Hobbs WR, Willis JK (2013) Midlatitude north atlantic heat transport: A time series based on satellite and drifter data. J Geophys Res 117:C01,008, doi:10.1029/2011JC007,039

Johns WE, Baringer MO, Beal LM, Kanzow SACT, Bryden HL, Hirschi JJM, Marotzke J, Meinen CS, Shaw B, Curry R (2011) Continuous, array-based estimates of Atlantic Ocean heat transport at 26.5°N. J Climate 24(10):2429–2449

Josey SA, Grist JP, Marsh R (2009) Estimates of meridional overturning circulation variability in the North Atlantic from surface density flux fields. journal of Geophysical Research 114:C09,022, doi:10.1029/2008JC005,230

Kanzow T, Cunningham SA, Johns WE, Hirschi JJM, Marotzke J, Baringer MO, Meinen CS, Chidichimo MP, Atkinson C, Beal LM, Bryden HL, Collins J (2010) Seasonal variability of the Atlantic Meridional Overturning Circulation at 26.5°N. J Climate 23:5678–5698

Keenlyside NS, Latif M, Jungclaus J, Kornblueh L, Roeckner E (2008) Advancing decadal-scale climate prediction in the North Atlantic sector. Nature 453:doi:10.1038/nature06,921

Klotzbach PJ, Gray WM (2008) Multidecadal variability in North Atlantic tropical cyclone activity. J Clim 21:3929–3935

Knight JR, Folland CK, Scaife AA (2006) Climate impacts of the Atlantic multidecadal oscillation. Geoph Res Lett 33:L17,706, doi:10.1029/2006GL026,242

LaRow TE, Stefanova L, Shin DW, Cocke S (2010) Seasonal Atlantic tropical cyclone hindcasting/forecasting using two sea surface temperature datasets. Geophys Res Lett 37:L02,804, doi:10.1029/2009GL041,459

Latif M, Roeckner E, Botzet M, Esch M, Haak H, Hagemann S, Jungclaus J, Legutke S, Marsland S, Mikolajewicz U, Mitchell J (2004) Reconstructing, monitoring, and predicting decadal-scale changes in the North Atlantic thermohaline circulation with sea surface temperature. Science 17:16051614

Matei D, Baehr J, Jungclaus JH, Haak H, Mller WA, Marotzke J (2012) Multiyear prediction of monthly mean Atlantic Meridional Overturning Circulation at 26.5°N. Science 335

Maury MF (1855) The physical geography of the sea and its meteorology. Harper and Brothers, New York

McCarthy G, Frajka-Williams E, Johns W, Baringer M, Meinen CS, Bryden HL, Rayner D, Duchez A, Cunningham SA (2012) Observed interannual variability of the Atlantic Meridional Overturning Circulation at 26.5°N. Geophys Res Lett 39:L19,609

McCarthy GD, Smeed DA, Johns WE, Frajka-Williams E, Moat BI, Rayner D, Baringer MO, Meinen CS, Collins J, Bryden HL (2014) Measuring the atlantic meridional overturning circulation at 26°N. Progress in Oceanography 130:91–111

McCarthy GD, Smeed DA, Johns WE, Frajka-Williams E, Moat BI, Rayner D, Baringer MO, Meinen CS, Collins J, Bryden HL (2015) Ocean impact on decadal Atlantic climate variability revealed by sea–level observations. Nature 521:508–510

Mielke C, Frajka-Williams E, Baehr J (2013) Observed and simulated variability of the AMOC at 26°N and 41°N. Geophysical Research Letters 40:11591164 doi:10.1002/grl.50,233

Msadek R, Dixon KW, Delworth TL, Hurlin W (2010) Assessing the predictability of the atlantic meridional overturning circulation and associated fingerprints. Geophysical Research Letters 37(19), l19608

Persechino A, Mignot J, Swingedouw D, Guilyardi E (2013) Decadal predictability of the Atlantic Meridional Overturning Circulation and Climate in the IPSL-CM5A-LR model. Clim Dyn pp doi: 10.1007/s00,382–012–1466–1

Pohlmann H, Smith DM, Balmaseda MA, Keenlyside NS, Masina S, Matei D, Mller WA, Rogel P (2013) Predictability of the mid–latitude Atlantic meridional overturning circulation in a multi–model system. Clim Dyn pp 41–775785. doi: 10.1007/s00,382–013–1663–6

Preisendorfer (1988) Principal Component Analysis in Meteorology and Oceanography. Elsevier, Amsterdam, 425p.

Reynolds RW, Smith TM, Liu C, Chelton DB, Casey KS, Schlax MG (2007) Daily high-resolution blended analyses for sea surface temperature. J Climate 20:5473–5496

Roberts CD, Garry FK, Jackson LC (2013) A Multimodel Study of Sea Surface Temperature and Subsurface Density Fingerprints of the Atlantic Meridional Overturning Circulation. J Clim 26:9155–9174

Robson JI, Sutton RT, Smith DM (2012a) Initialized decadal predictions of the rapid warming of the North Atlantic Ocean in the mid 1990s. Geophys Res Lett 39:L19,713, doi:10.1029/2012GL053,370

Robson JI, Sutton RT, Smith DM, Lohmann K, Smith D, Palmer MD (2012b) Causes of the Rapid Warming of the North Atlantic Ocean in the Mid-1990s. J Climate 25:4116–4134.

Robson JI, Sutton RT, Smith DM (2014) Decadal predictions of the cooling and freshening of the North Atlantic in the 1960s and the role of ocean circulation. Clim Dyn 42:2353–2365, DOI 10.1007/s00,382–014–2115–7

Roemmich D, Wunsch C (1985) Two transatlantic sections:Meridional circulation and heat flux in the subtropical North Atlantic Ocean. Deep-Sea Res Part a 32:619–644

Saunders MA, Lea AS (2008) Large contribution of sea surface warming to recent increase in atlantic hurricane activity. Nature 451:C03,021, doi:10.1038/nature06,422

Schneider EK, Fan M (2012) Observed decadal North Atlantic tripole SST variability. Part II: Diagnosis of mechanisms. J Atmos Sci 69:51–64

Seager R, Kushnir Y, Visbeck M, Naik N, Miller J, Cullen GKH (2000) Causes of Atlantic Ocean climate variability between 1958 and 1998. J Climate 13:2845–2862

Sévellec F, Fedorov AV (2014) Millennial Variability in an idealized ocean model: predicting the AMOC regime shifts. J Climate 27(10):3551–3564, doi:10.1175/JCLI–D–13–00,450.1

Smeed DA, McCarthy G, Cunningham SA, Frajka-Williams E, Rayner D, Johns WE, Meinen CS, Baringer MO, Moat BI, Duchez A, Bryden HL (2014) Observed decline of the Atlantic Meridional Overturning Circulation 2004 to 2012. Ocean Sci, 10:29–38, doi:10.5194/os–10–29–2014

Solomon S, Qin D, Manning M, Chen Z, Marquis M, Averyt KB, Tignor M, H L Miller e (2007) The Physical Science Basis. Contribution of Working Group I to the Fourth Assessment Report of the Intergovernmental Panel on Climate Change. Cambridge University Press, Cambridge, United Kingdom and New York, NY, USA pp ISBN 978–0–

521–88,009–1 (pb: 978–0–521–70,596–7)

Sonnewald M, Hirschi JJM, Marsh R, McDonagh EL, King BA (2013) Atlantic meridional ocean heat transport at 26°N: impact on subtropical ocean heat content variability. Ocean Sci 9:1057–1069

Sriver R, Huber M (2007) Observational evidence for an ocean heat pump induced by tropical cyclones. Nature 447:doi:10.1038/nature05,785

Stocker TF, Qin D, Plattner GK, Tignor M, Allen S, Boschung J, Nauels A, Xia Y, Bex V, (eds) PM (2013) The Physical Science Basis. Contribution of Working Group I to the Fifth Assessment Report of the Intergovernmental Panel on Climate Change. Cambridge University Press, Cambridge, United Kingdom and New York, NY, USA pp 1535 pp, doi:10.1017/CBO9781107415,324

Stouffer R, Yin J, Gregory JM, Dixon KW, Spelman MJ, Hurlin W, Weaver AJ, Eby M, Flato GM, Hasumi H, Hu A, Jungclaus JH, Kamenkovich IV, Levermann A, Monotoya M, Murakami S, Nawrath S, Oka A, Peltier WR, Robitaille DY, Sokolov A, Vettoretti G, Weber SL (2005) Investigating the causes of the response of the thermohaline circulation to past and future climate changes. Journal of Climate 19:1365–1387

Strazzo S, Elsner JB, Trepanier JC, Emanuel KA (2013) Frequency, intensity, and sensitivity to sea surface temperature of North Atlantic tropical cyclones in best-track and simulated data. J Adv Model Earth Syst 5:doi:10.1002/jame.20,036

Sutton RT, Dong B (2012) Atlantic Ocean influence on a shift in European climate in the 1990s. Nature Geoscience 5:788–792

Taws SL, Marsh R, Wells NC, Hirschi J (2011) Upper ocean manifestations of a reducing meridional overturning circulation. Geophys Res Lett 38:L20,601, doi:10.1029/2011GL048,978

Trenberth K, Caron J (2001) Estimates of meridional atmosphere and ocean heat transports. J Climate 14:3433–3443

Trenberth KE, Shea DJ (2006) Atlantic hurricanes and natural variability in 2005. Geophysical Research Letter 33:L12,704, doi:10.1029/2006GL026,894,

Vecchi GA, Zhao M, Wang H, Villarini G, Rosati A, Kumar A, Held IM, Gudgel R (2011) Statistical-Dynamical Predictions of Seasonal North Atlantic Hurricane Activity. Mon Wea Rev 139:1070–1082

Winton M (2003) On the climatic impact of ocean circulation. J Climate 16:2875–2889

Wunsch C (2005) The total meridional heat flux and its oceanic and atmospheric partition. J Climate 18:4374–4380

Zhang R, Delworth TL (2006) Impact of Atlantic multidecadal oscillations on India/Sahel rainfall and Atlantic hurricanes. Geophys Res Lett, 33:L17,712, doi:10.1029/2006GL026,267